Draft version February 2, 2008
Preprint typeset using LaTeX style emulateapj v. 9/08/03

arXiv:astro-ph/0401413v1 21 Jan 2004

# CONSTRAINTS ON EARLY NUCLEOSYNTHESIS FROM THE ABUNDANCE PATTERN OF A DAMPED LY$\alpha$ SYSTEM AT $z = 2.626$

Yeshe Fenner
Centre for Astrophysics & Supercomputing, Swinburne University, Hawthorn, Victoria, 3122, Australia and
UCO/Lick Observatory, University of California, Santa Cruz; Santa Cruz, CA 95064

Jason X. Prochaska
UCO/Lick Observatory, University of California, Santa Cruz; Santa Cruz, CA 95064

and

Brad K. Gibson
Centre for Astrophysics & Supercomputing, Swinburne University, Hawthorn, Victoria, 3122, Australia
*Draft version February 2, 2008*

## ABSTRACT

We have investigated chemical evolution in the young universe by analysing the detailed chemical enrichment pattern of a metal-rich galaxy at high redshift. The recent detection of over 20 elements in the gas-phase of a damped Lyman-$\alpha$ absorber (DLA) at $z = 2.626$ represents an exciting new avenue for exploring early nucleosynthesis. Given a strict upper age of $\sim 2.5$ Gyr and a gas-phase metallicity about one third solar, we have shown the DLA abundance pattern to be consistent with the predictions of a chemical evolution model in which the interstellar enrichment is dominated by massive stars with a small contribution from Type Ia supernovae. Discrepancies between the empirical data and the models are used to highlight outstanding issues in nucleosynthesis theory, including a tendency for Type II supernovae models to overestimate the magnitude of the "odd-even" effect at subsolar metallicities. Our results suggest a possible need for supplemental sources of magnesium and zinc, beyond that provided by massive stars.

*Subject headings:* galaxies: abundances — galaxies: chemical evolution — galaxies: intergalactic medium

## 1. INTRODUCTION

Chemical abundances in local stars are fossil evidence from which early nucleosynthetic processes may be inferred. An alternative probe into the earliest epochs of the universe is via the direct detection of metals in high redshift neutral gas. This requires a suitable background source such as a quasar, whose spectrum reveals absorption features in the intervening gas clouds. Damped Lyman-$\alpha$ Absorbers (DLAs) are one such class of quasar absorption system, defined as having an H I column density $N(\mathrm{H\,I}) \gtrsim 2 \times 10^{20}$ cm$^{-2}$.

The recent discovery of an intervening galaxy along the sightline to the quasar FJ081240.6+320808 (hereafter DLA-B/FJ0812+32) has lead to the most comprehensive abundance pattern measured beyond the local universe (Prochaska, Howk, & Wolfe 2003, hereafter PHW03). The gas-phase abundances of over 20 elements - including B, Cu, Ga, and Ge - have been detected in this galaxy, which has an unusually high column density and metallicity. Many of these elements have never before been measured at high redshift and provide a unique opportunity to probe early conditions of galaxy formation.

Identifying the modern-day counterparts to DLAs is still an open question. Kinematic evidence is consistent with DLAs being large protothick disks (Prochaska & Wolfe 1997) or smaller merging protogalactic clumps (Haehnelt et al. 1998), while chemical properties have lead others to favour intervening dwarf or irregular galaxies (e.g. Lanfranchi & Friaça 2003 and references therein). Galaxies giving rise to DLAs are likely to encompass a wide size and morphological range, from dwarf irregulars to giant ellipticals. Indeed, imaging studies of low redshift DLAs expose a variety of galactic types (e.g. Le Brun et al. 1997; Rao et al. 2003). Observed DLAs may tend to probe different types of galaxies at different evolutionary stages as a function of redshift.

The metal-line absorption profiles of the galaxy DLA-B/FJ0812+32 provide a snapshot of the chemical composition in the interstellar gas along only one sightline at one point in time. However a sufficiently detailed abundance pattern opens a window into the past history of star formation because chemical elements are produced on different characteristic timescales depending on their nucleosynthetic origin. The abundance of metals in the gas-phase of galaxies and protogalaxies reflects the interplay between processes including star formation, the synthesis of elements by stars, the release of metal-rich material via stellar winds and supernovae, and the flow of gas. We have constructed a range of simple chemical evolution models that follow these processes as a means of analysing this DLA. We discuss instances where the inability to correctly predict specific elemental abundances may indicate gaps in our understanding of nucleosynthesis.

In Section 2 we describe the observations of the DLA at $z = 2.626$ along the sight-line to FJ081240.6+320808, upon which this study is based. Section 3 describes the ingredients of the chemical evolution code used to model this DLA. In Section 4 the theoretical predictions are compared with the DLA data and we discuss the sensitivity of the results to age, metallicity, and model ingredients.

## 2. OBSERVATIONS

DLA-B/FJ0812+32 was identified in the discovery spectra of the FIRST Bright Quasar Survey (White et al. 2000). Subsequent $R \approx 8000$ spectroscopy with the ESI spectrometer (Sheinis et al. 2002) revealed its very strong metal-line

Electronic address: yfenner@astro.swin.edu.au
Electronic address: yfenner@astro.swin.edu.au

TABLE 1
ELEMENTAL ABUNDANCES IN DLA-B/FJ0812+32 [a]

| El | [X/H][b] | $\sigma_N^c$ | $\delta_{DC}$(90% c.l.)[d] | [X/S][e] |
|---|---|---|---|---|
| B | −0.57 | 0.085 | 0.1 (0.05) | +0.3 |
| N | > −2.24 | 0.058 | 0.0 (0.1) | > −1.47 |
| O | −0.54 | 0.101 | 0.1 (0.05) | +0.33 |
| Mg | −0.78 | 0.053 | 0.3 (0.1) | +0.29 |
| Al | > −2.00 | 0.054 | > 0.5 | > −0.73 |
| Si | −0.91 | 0.053 | 0.3 (0.1) | +0.16 |
| P | < −1.06 | 0.000 | < 0.3 | < +0.01 |
| S | −0.87 | 0.050 | 0.1 (0.05) | 0.0 |
| Cl | −1.55 | 0.000 | > 0.0 | > −0.78 |
| Ti | −1.87 | 0.112 | > 0.7 | > −0.4 |
| Cr | −1.61 | 0.032 | > 0.7 | > −0.14 |
| Mn | < −1.85 | 0.000 | 0.7 (0.1) | < −0.38 |
| Fe | −1.69 | 0.017 | > 0.7 | > −0.22 |
| Co | < −1.48 | 0.000 | > 0.7 | > −0.01 |
| Ni | −1.73 | 0.007 | > 0.7 | > −0.26 |
| Cu | < −1.11 | 0.000 | > 0.7 | < +0.36 |
| Zn | −0.91 | 0.022 | 0.2 (0.1) | +0.06 |
| Ga | < −1.45 | 0.000 | 0.7 (0.1) | < +0.02 |
| Ge | −0.92 | 0.035 | 0.3 (0.1) | +0.15 |
| As | < 0.26 | 0.000 | 0.0 | < +1.03 |
| Kr | < −0.44 | 0.000 | 0.0 (0.1) | < +0.33 |
| Sn | < −0.27 | 0.000 | 0.0 (0.1) | < +0.5 |
| Pb | < −0.10 | 0.000 | 0.0 (0.1) | < +0.67 |

[a] Measurements taken by Prochaska, Howk, & Wolfe (2003).
[b] Gas-phase abundance on a logarithmic scale relative to solar, where $N(\mathrm{HI}) = 10^{21.35}$ cm$^{-2}$.
[c] Statistical error on gas-phase abundances.
[d] Dust-corrections and uncertainties estimated from depletions patterns observed in Galactic gas.
[e] Dust-corrected abundances on a logarithmic scale relative to S.

transitions (Prochaska et al. 2003). PHW03 published HIRES echelle spectra of this 'metal-rich' DLA and reported the detection of over 20 elements. The resulting abundance pattern provides an unparalleled laboratory for the study of elemental production in the young universe.

PHW03 derived gas-phase abundances using standard techniques and estimated uncertainties in the measurements by propagating the statistical errors. With only a few exceptions, the dominant uncertainty in the resulting elemental abundances is the effect of differential depletion. Similar to the ISM of the Milky Way, refractory elements like Ni, Fe, Cr may be depleted from the gas-phase such that their observed abundances are significantly lower than their intrinsic values. This is the principal challenge to studying chemical abundances in the DLA and it has led to competing interpretations of their chemical evolution history (e.g. Lu et al. 1996; Kulkarni, Fall, & Truran 1997; Prochaska & Wolfe 2002; Vladilo 2002). In the following analysis, we adopt the conservative dust corrections imposed by PHW03 based on empirical depletion patterns observed for the Milky Way ISM (e.g. Savage & Sembach 1996). Table 1 lists both the gas-phase abundances and dust-corrected abundance ratios for the elements observed in DLA-B/FJ0812+32 by PHW03, along with statistical errors and dust-correction factors. When relevant, we discuss the implications of dust depletion for our conclusions. Further detail regarding the observational errors will be given in Prochaska et al. (2003, in preparation).

## 3. THE MODEL

We simulated the chemical enrichment history of a DLA using the chemical evolution code described in Fenner & Gibson (2003). Under this formalism, primordial gas is allowed to collect and form stars that synthesise new elements. An exponentially decaying gas infall rate was adopted and there were no outflows of gas driven by galactic winds. In this way, the models described below resemble different regions of disk galaxies. The evolution of the gas phase abundance pattern reflects the cumulative history of the dynamic processes of star formation, stellar evolution, and nucleosynthesis. The classic set of equations governing these processes (described in the seminal work of Tinsley 1980), have been numerically solved by defining $\sigma_i(t)$ as the mass surface density of species $i$ at time $t$, and assuming that the rate of change of $\sigma_i(t)$ is given by:

$$\frac{d}{dt}\sigma_i(t) = \int_{m_{low}}^{m_{up}} \psi(t-\tau_m)\, Y_i(m, Z(t-\tau_m))\, \frac{\phi(m)}{m}\; dm + \frac{d}{dt}\sigma_i(t)_{infall} - X_i(t)\,\psi(t), \quad (1)$$

where the three terms on the right-hand side of equation (1) correspond to the stellar ejecta, gas infall, and star formation, respectively. $\psi$ is the SFR, $Y_i(m, Z(t-\tau_m))$ is the stellar yield of $i$ (in mass units) from a star of mass $m$ and metallicity $Z(t-\tau_m)$, $\phi(m)$ is the initial mass function, and $X_i$ is the mass fraction of element $i$. By definition, the sum of $X_i$ over all $i$ is unity, and the total surface mass density is identical to the integral over the infall rate. $m_{low}$ and $m_{up}$ are the lower and upper stellar mass limits, respectively, and $\tau_m$ is the main-sequence lifetime of a star of mass $m$. In practice, the first term is split into three equations that deal separately with low-mass stars, Type Ia supernova (SN) progenitors, and massive stars.

We now describe each of the model ingredients in turn, distinguishing the inputs that are parameterised using simple analytical prescriptions from the nucleosynthesis inputs, which are derived numerically from first principles.

### 3.1. *Analytical Prescriptions*

*Initial Mass Function (IMF):* The initial mass function determines the relative birth rate of stars as a function of mass. Because different mass stars leave unique chemical signatures on the ISM and operate on different characteristic timescales, the precise form of the IMF is a key factor driving the evolution of abundance ratios. This model assumed the Kroupa, Tout, & Gilmore (1993) three component IMF. The Kroupa et al. function has fewer stars in the low and high mass ends of the distribution than the single power-law Salpeter (1955) function. In Section 4.2.4 we estimate the sensitivity of the results to changes in the upper mass limit of the IMF.

*Star Formation Rate (SFR):* A simple analytical law for the SFR was adopted. Akin to the Schmidt (1959) law, we varied the SFR in proportion to the square of gas surface density. The efficiency of star formation was adjusted in order to investigate different timescales for metal enrichment.

*Infall Rate:* The gas infall rate was assumed to decay exponentially on timescales ranging between 3 and 9 Gyr. For the same final metallicity, a shorter infall timescale corresponds to a younger object. The star formation efficiency was also assumed to be higher in the models that became metal-enriched the fastest - this is motivated by the expectation that a deeper potential well corresponds to a faster rate of collapse and a higher efficiency of star formation. We note that it is the combination of both infall rate and star formation efficiency that is of foremost importance and these two effects determine the time taken to reach a specific metallicity. In the present study, the timescale for metal enrichment is more important than either the infall timescale or star formation efficiency

considered in isolation. For this reason, we present results as a function of age and base our discussion on "age-sensitivity".

### 3.2. *Stellar Yields and Lifetimes*

*Intermediate and low mass stars:* We incorporate the results of van den Hoek & Groenewegen (1997) whose metallicity-dependent yields are specified over the mass range 0.9–8 $M_\odot$. These stars are integral in the synthesis of C and N, however observational constraints for these two elements are lacking for DLA-B/FJ0812+32. Thus this stellar population will be largely ignored in the following discussions. Low-mass stars may be the principle production site for Galactic Pb (Travaglio et al. 2001) as well as producing modest quantities of As, Kr, and Sn via s-process nucleosynthesis. The abundance of these s-process elements may prove to be sensitive indicators of age in high redshift protogalaxies because they are generated in 1−4 $M_\odot$ stars with typical lifetimes between a few hundred Myr and a few Gyr. However, remaining uncertainties in the theory of the s-process, as well as observational complications regarding s-element contamination by companions stars, may limit the use of Pb as an age indicator. An investigation into s-process enrichment in DLAs will be the focus of a forthcoming paper.

*Type Ia supernovae (SNe Ia):* A recalculation of the 1986 W7 model (Thielemann, Nomoto, & Yokoi 1986) by Iwamoto et al. (1999) was adopted. About 0.75 $M_\odot$ of iron is ejected per event. Our model assumed that 3% of binary systems involving intermediate and low mass stars result in SNe Ia. This fraction provides a good fit for the solar neighbourhood (e.g. Alibés, Labay, & Canal 2001; Fenner & Gibson 2003).

*Massive stars:* Stars more massive than $8 - 10$ $M_\odot$ that end their lives in violent supernova explosions are responsible for most of the metals in the cosmos. We investigated chemical evolution using two different sets of SN II yields: 1) the Woosley & Weaver grid (1995, hereafter WW95) covering a mass range 11–40 $M_\odot$; and 2) a set of 36 Type II SNe models covering the mass range 11–40 $M_\odot$ at six metallicities (Z = 0, $10^{-6}$, $10^{-4}$, $10^{-3}$, $6 \times 10^{-3}$, $2 \times 10^{-2}$) recently compiled by Limongi & Chieffi (2003, hereafter FRANEC) using the latest version of the FRANEC code described in Limongi & Chieffi (2002).

For WW95, we took the lower energy "A" models for stars $\leq$ 25 and the higher energy "B" models for heavier stars. Taking note of the suggestion by Timmes, Woosley, & Weaver (1995) that the WW95 mass cuts may have penetrated too deeply within the iron core, we have uniformly halved the iron yields from these models [1]. The FRANEC models all have arbitrary mass cuts corresponding to 0.09–0.1 $M_\odot$ of $^{56}$Ni.

The nucleosynthesis models only extend to 40 and 35 $M_\odot$ for WW95 and FRANEC, respectively. Since stars as heavy as 100 $M_\odot$ are permitted to form in our chemical evolution model (albeit ten times less frequently than 40 $M_\odot$ counterparts), the predicted yields were linearly extrapolated for stars outside the mass grid. Section 4.2.4 discusses the sensitivity of the results to the assumed upper mass limit on the formation of stars.

Unless otherwise stated, subsequent comparison between theoretical and observed elemental abundances will refer to the models calculated using WW95. In Section 4.2.5 we show that while WW95 and FRANEC make very different predictions regarding the magnitude of the "odd-even" effect, for most of the elements between O and Ni, for which DLA measurements exist, our conclusions drawn from the WW95 models also apply to the FRANEC models.

*Stellar lifetimes:* We adopt metallicity-dependent main-sequence (MS) lifetimes calculated by Schaller et al. (1992). Stars pollute the interstellar medium with metals over the course of their evolution via stellar winds and planetary nebulae, however this model assumes that all the mass loss takes place at the end of the MS phase. This simplification is not expected to influence our predictions, since the enrichment pattern is mostly controlled by massive stars whose metals are returned to the ISM almost entirely during the supernova explosion.

As a word of caution, this type of model assumes that stellar ejecta is uniformly mixed into the gas phase and therefore predicts *mean* abundance trends. In reality, the products of SNe not only mix inhomogeneously with the ambient gas, but may also be associated with regions in different ionisation states. Despite these caveats, a homogeneous chemical evolution model is a reasonable representation of this DLA for several reasons: firstly, the measured enrichment pattern of this $z = 2.626$ object reflects the average in the gas phase along a line-of-sight; secondly, in order to reach a metallicity of $\sim 1/3$ solar, numerous generations of supernovae must have exploded, which will tend to "smooth out" the spatial distribution of the heavy elements; and, thirdly, similar to the majority of DLA (Prochaska 2003) there are only modest variations in the relative abundances of the DLA across the observed velocity profile. These small variations are likely associated to differences in differential depletion implying a chemically homogeneous system.

## 4. RESULTS

### 4.1. *Model versus Data*

Figure 1 presents the difference between the observed DLA enrichment pattern and the predicted [X/S][2] from our fiducial WW95 model that reaches [O/H] = −0.44 after 2.2 Gyr. The dashed line indicates perfect agreement between the model and the data, while the dotted lines represent a factor of two difference. We conservatively consider predictions falling within the dotted lines to be acceptable. The arrows denote the direction in which the difference will move if the observational limits tighten. For elements like Fe, Ni, and Cr, the lower limits are set by dust depletion and are unlikely to change. Error bars reflect statistical errors on gas-phase abundance measurements, where the statistical error on [X/S] equals the quadrature sum of the statistical errors on [X/H] and [S/H] given in Table 1. When not reported as limits, uncertainties in the dust corrections range from from 0.05 to 0.1 dex, i.e. comparable to the magnitude of the statistical errors.

There is excellent agreement between the fiducial model and the DLA data for most elements from B to Ge. This agreement is particularly impressive given that the models we are applying to a high redshift object were tuned using local stellar abundance patterns. Part of the explanation is that the DLA pattern is close to solar. Nevertheless, the models match an observed trend in the $\alpha$-elements of decreasing [X/S] with increasing atomic number (Figure 2). Furthermore, the model reproduces the mildly enhanced "odd-even" effect indicated by the limits to the Al, P, and Cl abundances. There is also good agreement for the iron-peak elements Cr, Mn, Fe and Co and the heavier r-process elements Ga and Ge. The Ni and Cu predictions do not violate the observational limits. The most serious disagreement occurs for Mg and Zn,

[1] We note that this violates the self-consistency of the stellar models, since a shift in mass cut that halves the Fe yield is expected to also modify the yield of elements like Co and Ni.

[2] We do not use Fe as the reference element because its nucleosynthesis is subject to many uncertainties relating to the SN II mass cut and the evolution of the SN Ia rate. Oxygen has a more robust theory of production, but its observational status and solar abundance is less certain. Thus we plot abundances relative to sulfur, for which an ample database of DLA and stellar measurements exists. Moreover, the nucleosynthetic origin of S is thought to be well understood - being mainly generated by hydrostatic burning and explosive O and Si burning in massive stars.

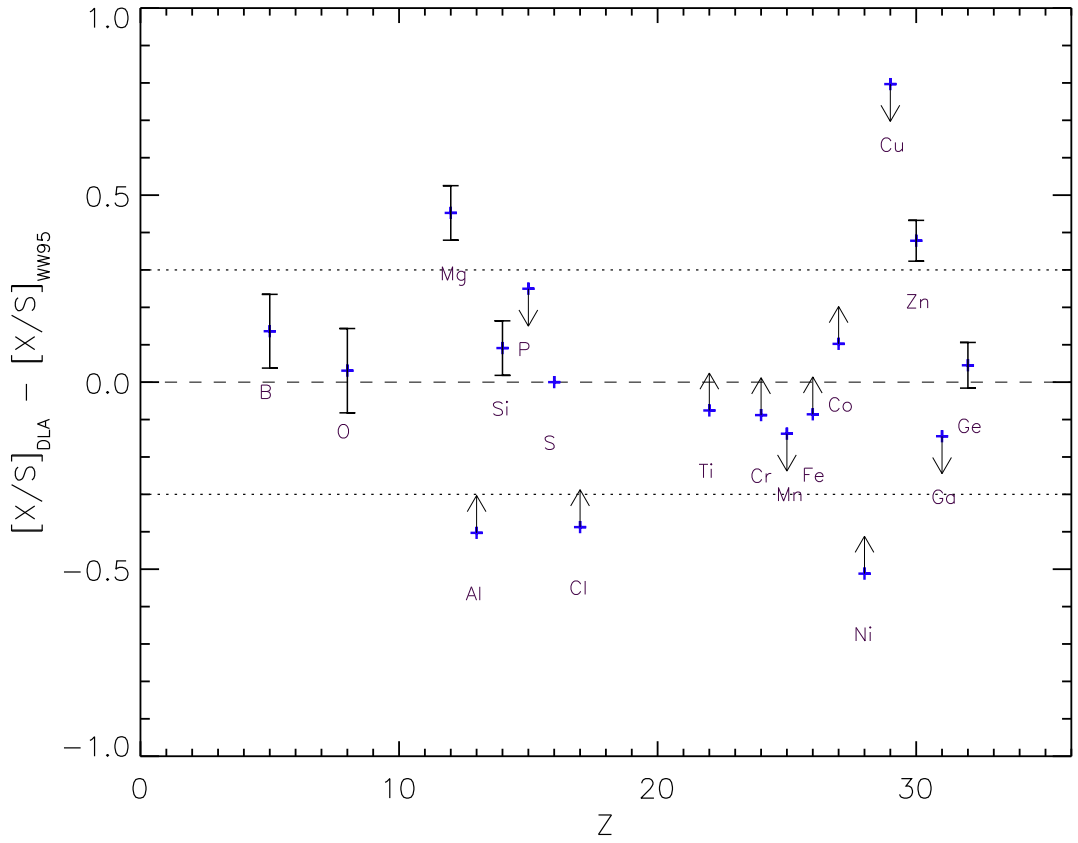


FIG. 1.— Logarithmic ratio of the observed and predicted DLA abundance pattern using Woosley & Weaver 1995 SN II yields for a 2.2 Gyr model with [O/H] = −0.44. Arrows indicate the direction in which the difference will move if the upper and lower observational limits tighten. For elements like Fe, Ni, and Cr, the lower limits are set by dust depletion and are unlikely to change. Error bars reflect statistical errors on gas-phase abundance measurements. The level of uncertainty in the dust correction factor is comparable to the statistical errors. The dashed line indicates agreement between observations and predictions, while the dotted lines denote deviations of a factor of two.

which are underpredicted by the model by about 0.45 and 0.4 dex, respectively. Detailed discussions of these elements are found in Sections 4.3.2 and 4.3.5.

### 4.2. *Model Sensitivity*

#### 4.2.1. *Dependence on Age*

Figure 2 presents the predicted abundance pattern for a model galaxy reaching a final metallicity of [O/H] = −0.44 after four different periods: 0.46, 0.9, 1.6, and 2.66 Gyr. The dust-corrected DLA abundance pattern (as presented in column 5 of Table 1) is indicated by black circles, with arrows specifying the upper and lower limits, where applicable. Upper limits on As, Kr, Sn, and Pb are shown, although their evolution is not modelled. Abundances are on a solar logarithmic scale relative to sulfur. The dashed line corresponds to the solar pattern and the dotted lines are deviations by a factor of two. The detection of and limits placed on 23 elements from B to Pb reveal a roughly solar-like enrichment pattern. This may not come as a surprise given the moderate metallicity of the object. However the redshift of this galaxy imposes an upper age limit of $\sim$ 2.5 Gyr, implying a much shorter timescale for metal-enrichment than in the solar neighbourhood.

The abundance of most elements relative to sulfur is virtually constant over the age range shown in Figure 2. This is because the enrichment pattern is mostly set by short-lived massive stars. The exceptions are carbon, nitrogen, and the iron-peak elements where modest differences are predicted. Low and intermediate mass stars have long been held to dominate the production of N and possibly that of C, although theoretical (e.g. Carigi 2000) and observational (e.g. Henry, Edmunds, & Köppen 2000) studies also support a strong contribution to C abundance from Type II SNe. Considerable synthesis of C, by the triple-alpha reaction of helium and N, via CNO processing, takes place within low and intermediate mass stars, which are longer lived than SN II progenitors. Hence the enrichment of the interstellar medium with C and N is delayed with respect to products of massive star nucleosynthesis. We stress that the results presented in this paper are largely insensitive to age.

The main deviation from the solar pattern is the mild enhancement of the alpha-elements O, Mg and Si with respect to Fe or Zn. There is also a trend toward lower relative abundances of $\alpha$-elements with higher atomic numbers. Massive, short-lived stars culminating in Type II SNe are the primary source of the alpha-elements, while Fe is produced in significant amounts by Type Ia SNe, whose lower mass progenitors have longer main-sequence lifetimes. Similar alpha-enhancement is also seen in halo and thick disk stars where it is understood to signify rapid star formation, whereby most stars formed from gas that had not yet been polluted with iron-rich SN Ia ejecta. Indeed, the ratio of iron-peak elements to sulfur is 30-60% higher in the 2.66 Gyr model compared with the 0.46 Gyr model.

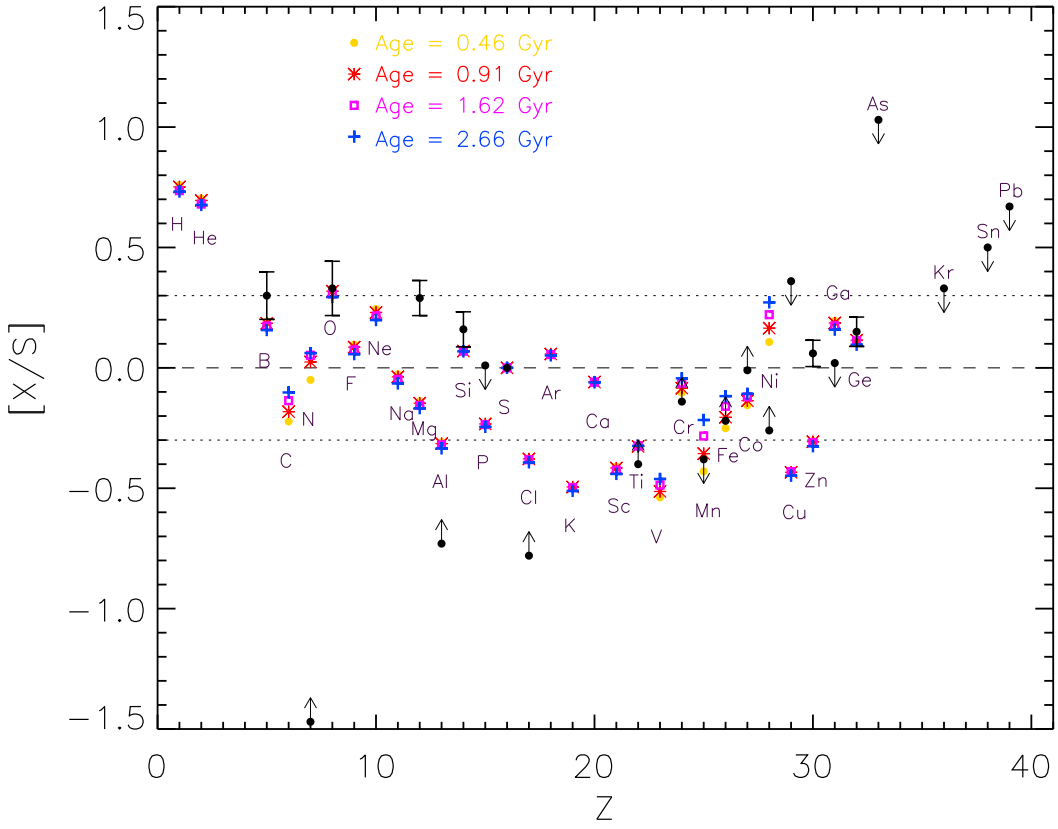


FIG. 2.— Predicted abundance pattern as a function of age. [O/H] = −0.44 in each model. Abundances are expressed relative to solar and scaled to sulfur, such that $[X/S] = \log_{10}(m(X)/m(S)) - \log_{10}(m(X)/m(S))_{\odot}$. Four ages ranging from 0.46 - 2.66 Gyr are represented by the symbols indicated. The dust corrected DLA abundance pattern is indicated by black circles. Statistical errors on the gas-phase abundance are indicated by error bars. Arrows reflect the corresponding lower and upper limits. The dotted lines indicate deviations from scaled solar by a factor of two.

It is apparent from Figure 2 that a protogalaxy that has reached 1/3 solar metallicity on a timescale of order 1 Gyr has already been contaminated by the nucleosynthetic products of intermediate mass stars and Type Ia SNe. This is because intermediate mass stars and SN Ia progenitors can have lifetimes as short as a few hundred Myr. Although the relative abundances of C, N, and the iron-peak elements exhibit moderate age sensitivity in Figure 2, a better probe of age in an intermediate redshift protogalaxy might be s-process elements such as Kr and Pb, since their origin in low mass stars should ensure an enrichment timescale in excess of $\sim$ 1 Gyr (Travaglio et al. 2001). A preliminary examination of Pb evolution indicates that [Pb/S] may increase by roughly an order of magnitude between 0.5 and 2.5 Gyr (Fenner et al. 2004, in preparation). The anticipated detection of s-process elements in additional DLAs may prove fruitful in constraining age.

#### 4.2.2. *The Role of Type Ia SNe*

Figure 2 reveals how the relative contribution from Type Ia SNe increases with the age of the object, for the same metallicity. Type Ia SNe are believed to be the chief source of the iron-peak elements. While the precise identity of SNe Ia progenitors is debated, they must involve intermediate to low mass stars in binary systems. The explosion occurs when a white dwarf in the binary system accretes enough material from its companion to exceed the Chandrasekhar limit. The timescale for the SN Ia event is thus determined by the evolution of the companion star. The characteristic timescale for SNe Ia is often taken to be 1 Gyr, however this is environment-dependent and moreover, the first Type Ia events may occur within only a few hundred Myr (Matteucci & Recchi 2001).

In theory, the iron-peak abundances might be used to constrain the age of this DLA. This requires assumptions to be made about the incidence of SNe Ia. As mentioned in Section 3.2, we have adopted the Milky Way value for the fraction of low and intermediate-mass binary systems that culminate in SNe Ia. In practice, there is a conflict between the predictions for Mn, which imply an age $\lesssim$ 1 Gyr and predictions for Fe, which imply that the protogalaxy has been forming stars for more than 1 Gyr. In other iron-peak elements, [Co/S] falls slightly below the lower limit in all models, while Cr and Ni predictions agree with the data.

From Figure 2, Mn appears to have a very strong dependence on the age of the simulated galaxy. According to the nucleosynthesis prescriptions adopted in this paper, SNe Ia play such a strong role in Mn production that their contribution exceeds that from SNe II after $\sim$ 2.5 Gyr. It has been stated that Timmes et al. (1995) claim Type Ia SNe to be unimportant contributors to Mn synthesis (e.g. Nissen et al. 2000), yet it is clear from Figures 4 and 5 from Timmes et al. (1995) that Type Ia SNe produce $\sim$50% of the solar Mn abundance. What Timmes et al. showed instead was that the same trend of [Mn/Fe] vs [Fe/H] can be obtained either with or without SNe Ia due to the strong metallicity-

dependence of the WW95 SN II Mn yields. However, SNe Ia are needed to reach the solar abundance. When the same nucleosynthesis prescriptions used in this paper are applied to the solar neighbourhood, we find that ∼75% of the solar Mn abundance originates from SNe Ia.

The tendency for Mn to be overpredicted in these DLA models may suggest that the main Mn source is metallicity-dependent. Other DLA systems have been observed for which [Si/Fe] ∼ 0 yet [Mn/Fe] is significantly subsolar (e.g. Pettini et al. 2000). Current nucleosynthesis models cannot explain such behaviour, since a solar Si/Fe ratio points to a Type Ia SN contribution, but this is not supported by the low Mn abundance, whose origin is understood to lie mostly in SNe Ia. A similar trend has been identified in stellar abundances of the Sagittarius dSph galaxy (McWilliam, Rich, & Smecker-Hane 2003). Invoking metallicity-dependent SNe Ia Mn yields might help explain these apparently incompatible observations.

In a handful of DLAs with low dust content, Pettini et al. (2000) discern no correlation between [Mn/Fe] and [Fe/H], even though a clear trend is apparent in local stars at all metallicities (Carretta et al. 2002). They attribute this to the varied histories and morphologies of the objects and suggest that a process in addition to Type II and Ia nucleosynthesis may operate to explain Mn enrichment.

It should be noted that the theoretical yields of Mn from WW95 do not have sufficient metallicity-dependence to account for the low [Mn/Fe] ratios observed in very metal-poor stars (e.g. Alibés, Labay, & Canal 2001). Furthermore, Co/Fe ratios up to four times higher than solar are detected in local stars below [Fe/H] ∼ −2.5 (Cayrel et al. 2003), in conflict with the expectations of SNe II models. Thus, it is likely that gaps remain in our understanding of the processes responsible for Mn and Co that limit the power of this model to constrain the DLA age using these elements.

#### 4.2.3. *Sensitivity to Metallicity*

The production of certain elements (particularly those with odd atomic numbers) by massive stars is a strong function of the initial stellar chemical composition. We examined the dependence of the predicted enrichment pattern on the model galaxy's metallicity. Figure 3 depicts results from three models reaching [O/H] = −0.24, −0.44, and −0.64 after 2.2 Gyr of star formation. The ± 0.2 dex variation in [O/H] reflects the uncertainty in the measured H I column density.

The model results displayed in Figure 3 reveal the so-called "odd-even" effect, whereby the underabundance of odd-numbered elements with respect to their even-numbered neighbours increases with decreasing metallicity. This effect is a signature of massive SNe from subsolar-metallicity stars. Figure 4 shows the production factors relative to S from the WW95 SN II models integrated over the Kroupa et al. (1993) IMF over the mass range 11-100 $M_\odot$. The odd-even effect persists from the zero to 1/10th solar metallicity WW95 models, with the trend reversing in the solar model. The strength of the odd-even effect in this DLA can be gauged by comparing abundances between pairs of neighbouring odd-Z and even-Z elements. Evidence for a mild odd-even effect comes from the ratios [P/Si] < −0.15, [Mn/Fe] < −0.16, and [Ga/Ge] < −0.13.

Even-elements behave as primary products in SNe II and their stellar yields are robust to the initial metallicity. Conversely, the ratios of odd-elements to S show spreads of typically ∼ 0.2 dex over the 0.4 dex range in [O/H]. The SNe II yield of odd-elements from fluorine to the iron-peak is understood to be sensitive to the neutron excess and therefore increases with the initial abundance of "seed" nuclei present in the star. Thus the ratio of odd-elements to S is highest in the [O/H] = −0.24 model.

Copper exhibits the greatest sensitivity to metallicity, with Cu/S having a stronger than linear dependence on O/H over the metallicity range considered. Thus [Cu/S] has the potential to indirectly constrain the metallicity and the H I column density. The upper limit on the Cu detection arises because of line blending. However the depletion of Cu onto dust grains reduces its abundance in the gas-phase. Accounting for these opposing effects, the intrinsic Cu abundance is likely to fall within 0.4 dex of the current upper limit. Only the highest metallicity models approach the Cu observation. The predicted [Zn/S] value, which is underproduced by ∼0.4 dex in the [O/H] = −0.44 model, is also in closer agreement with data for the highest metallicity model.

Abundances of the odd-elements Al, P, and Cl relative to S offer a probe into the nature of the "odd-even" effect. However, only lower (for Al and Cl) and upper limits (for P) exist at present in this DLA. These limits are currently not sufficiently restrictive to eliminate any of the three different metallicity models depicted in Figure 3. Owing to the strength of the Al II $\lambda$ 1670 line, only lower limits can be placed on the Al abundance in many DLAs, yet absorption-line systems present a unique opportunity to acquire empirical evidence for the metallicity-dependent behaviour of P and Cl, whose weak stellar spectral lines mean there is a paucity of data from local stars. A database of measurements of these elements in DLAs will help test the theoretical expectation that Cl, P, and Al follow similar evolutionary paths.

One might expect from the theoretical predictions shown in Figure 3 that improved observations of P and Cl will see both [P/S] and [Cl/S] converging toward ∼ −0.4. However, the abundance of Cl shown in these figures was derived from the Cl I transition, which is not the dominant ion. After correcting for ionisation, the true Cl abundance is likely more than 0.5 dex higher than the current lower limit. Even when these models are evolved to solar metallicity, Al and Cl are still underproduced by 0.1 and 0.3 dex, respectively; suggesting that the odd-even effect may be slightly exaggerated in the stellar models, or that intermediate-mass stars provide an additional source. It should be noted that the solar reference Cl abundance used in this paper is ∼ 0.15 dex higher than the Anders & Grevesse (1989) value.

Boron is synthesised in a variety of ways including neutrino-induced reactions in the shells of SNe II (the $\tau$-process) and cosmic ray spallation onto seed nuclei in the interstellar medium (Fields & Olives 1999). The relative importance of these processes is expected to vary with metallicity. The $\tau$-process should produce constant B/O regardless of metallicity, whereas a signature of the cosmic ray process would be B/O decreasing with decreasing metallicity. The WW95 models generate B via the $\tau$-process and the satisfactory agreement with the observed B/O ratio lends support to a $\tau$-process origin for B.

#### 4.2.4. *Sensitivity to the Stellar Initial Mass Function*

It has been estimated that uncertainties in the shape and limits of the IMF correspond to variations in the *absolute* elemental yields by a factor of 2 (Wang & Silk 1993). We have tested the sensitivity of our results to a change in the upper mass limit of the IMF from 100 to 40 $M_\odot$. Figure 5 plots the logarithmic ratio of the abundance pattern obtained in these two cases. The abundances of most elements relative to S are unchanged. Prominent exceptions are F, Ne, and Na, whose yields relative to S decrease by factors ranging from 3 - 5. [O/S] is also lower by ∼0.25 dex when the IMF is curtailed at 40 $M_\odot$. The magnitude of the offset reflects the dependence of elemental yield on stellar mass. The elements most affected by the shift in upper IMF limit are those whose yields increase most steeply with initial stellar mass. The possible future detection of F in this DLA may help constrain

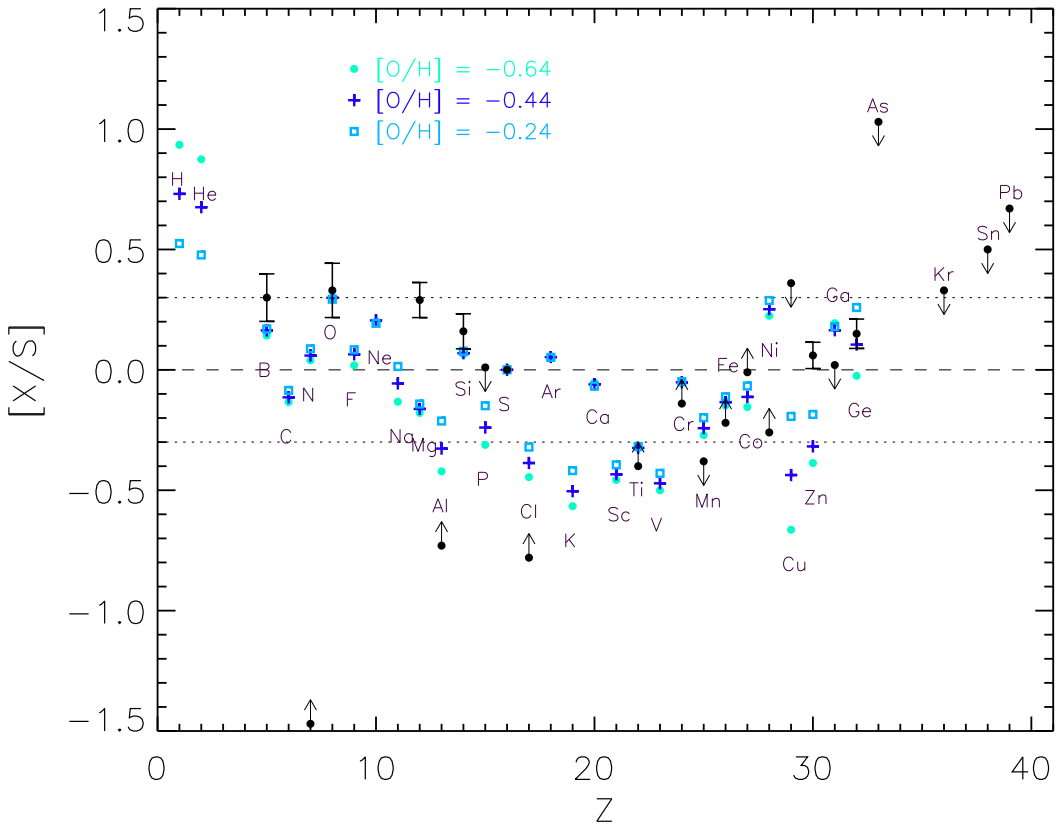


FIG. 3.— Predicted abundance pattern as a function of metallicity. The enrichment pattern for 2.2 Gyr model galaxies at [O/H] = −0.44 ± 0.2 are shown by the symbols indicated. Other symbols have the same meaning as in Figure 2.

the IMF.

#### 4.2.5. *Sensitivity to the Type II Supernova Nucleosynthesis Prescriptions*

Figure 6 compares the standard WW95 model with the same model using FRANEC yields for massive stars. We note several main differences: 1) B and F are produced in negligible amounts in the FRANEC model because neutrino-induced nucleosynthesis processes are omitted from their calculations; 2) the elements from Cu to Kr are present in trace amounts in the FRANEC model; and 3) the odd-even effect is much more pronounced in FRANEC models. In particular, P, Cl, K, and Sc are significantly lower with respect to S in the FRANEC model, whereas the abundance of their even-Z neighbours matches those from the WW95 model. The deficit of Cl from the FRANEC models with respect to the observations suggests that the odd-even effect may be too severe. Despite these differences, there is good consensus between the two models for about half of the elements with DLA measurements and many of the conclusions of this paper can be reached irrespective of the choice of SN II yields.

### 4.3. *Discussion of Individual Elements*

#### 4.3.1. *Oxygen*

In the most widely cited set of solar abundances from Anders & Grevesse (1989), the solar oxygen abundance was assumed to be $\log(N_O/N_H)_\odot + 12 = 8.93$. However, recent estimates that account for solar granulation and non-LTE effects lead to significant downward revisions in the Sun's oxygen abundance by almost a factor of two (to $\log(N_O/N_H)_\odot + 12 = 8.69$ - Allende Prieto, Lambert & Asplund 2001). Such a shift partly resolves the long-standing dichotomy between the Sun's oxygen abundance and that of the local ISM (André et al. 2003). This work adopts Holweger's (2001) preferred value of $\log(N_O/N_H)_\odot + 12 = 8.73$, whereas WW95 and FRANEC stellar yields were derived with the Anders & Grevesse (1989) values. Owing to uncertainties in stellar nucleosynthesis inputs such as the $^{12}C(\alpha,\gamma)^{16}O$ reaction rate, convection, and mass-loss (see Langer 1996; Gibson, Loewenstein, & Mushotzky 1997 for useful discussions of these uncertainties), we consider our predictions for the O abundance to be accurate within a factor of $\sim 2$.

#### 4.3.2. *Magnesium*

Figure 1 shows that the [Mg/S] value predicted by the standard model is 0.45 dex lower than is observed in this DLA. The reason is clear from Figure 4, which shows that Mg/S is slightly subsolar in the ejecta from a generation of WW95 metal-poor stars and tends toward the solar value at higher metallicity. The observed value of $[Mg/S]_{DLA} = +0.3$ dex cannot be matched by any single generation of WW95 stars and nor will any superposition of populations fit the data. Alibés et al. (2001) also found that WW95 yields lead to an underproduction of Mg in their models of the local disk; a problem which they suggest could be resolved if intermediate-mass stars or SNe Ia supply additional Mg. Indeed, $4 - 6\ M_\odot$ stars have been shown to contribute to most of the abundance of the neutron-rich Mg isotopes at low and intermediate metal-

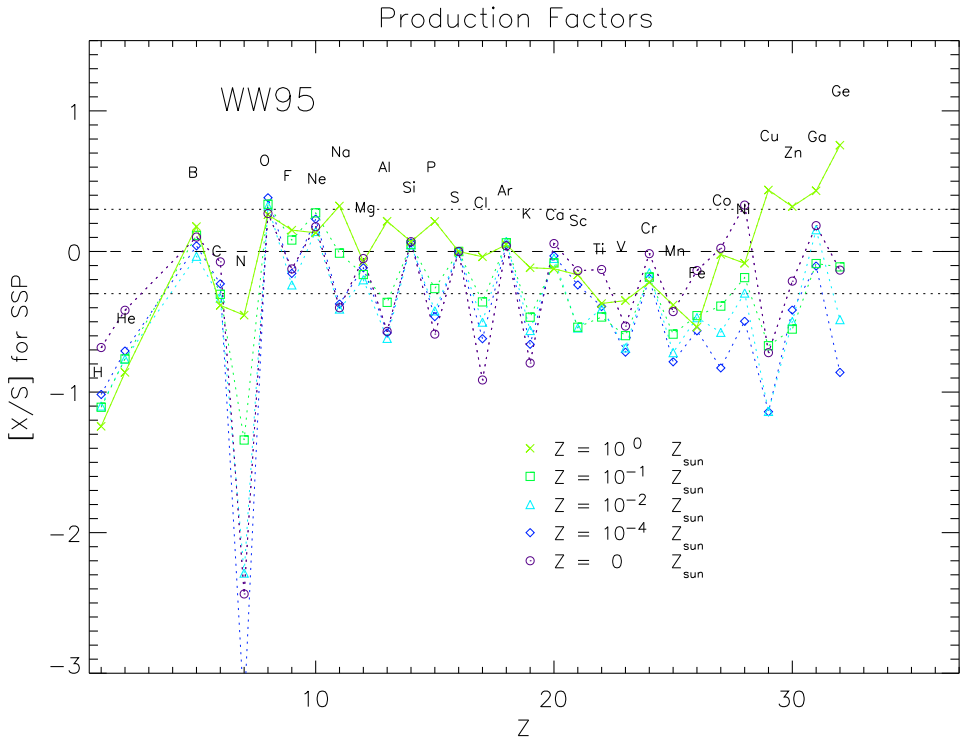


FIG. 4.— Production factors relative to S from a single generation of massive stars from 11–100 $M_\odot$ on a solar logarithmic scale using the yields of Woosley & Weaver 1995. Five metallicities are shown from zero to solar. C, N and some of the iron-peak elements are subsolar because they require additional sources such as intermediate- and low-mass stars and Type Ia SNe.

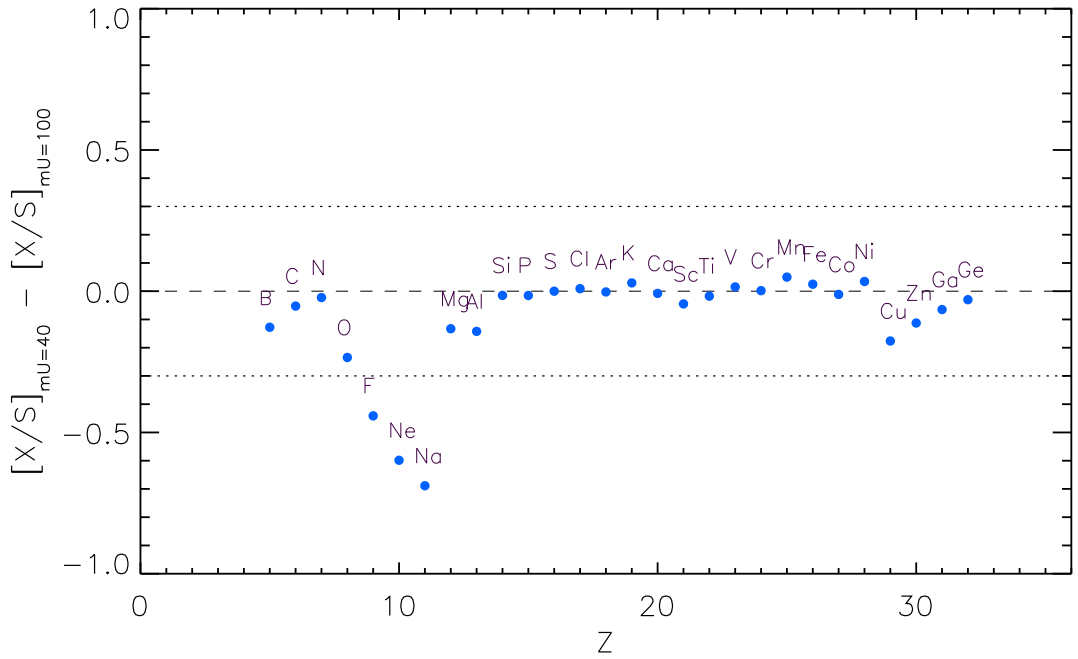


FIG. 5.— Logarithmic ratio of the abundance pattern obtained with an IMF upper limit of 40 $M_\odot$ and with an upper limit of 100 $M_\odot$.

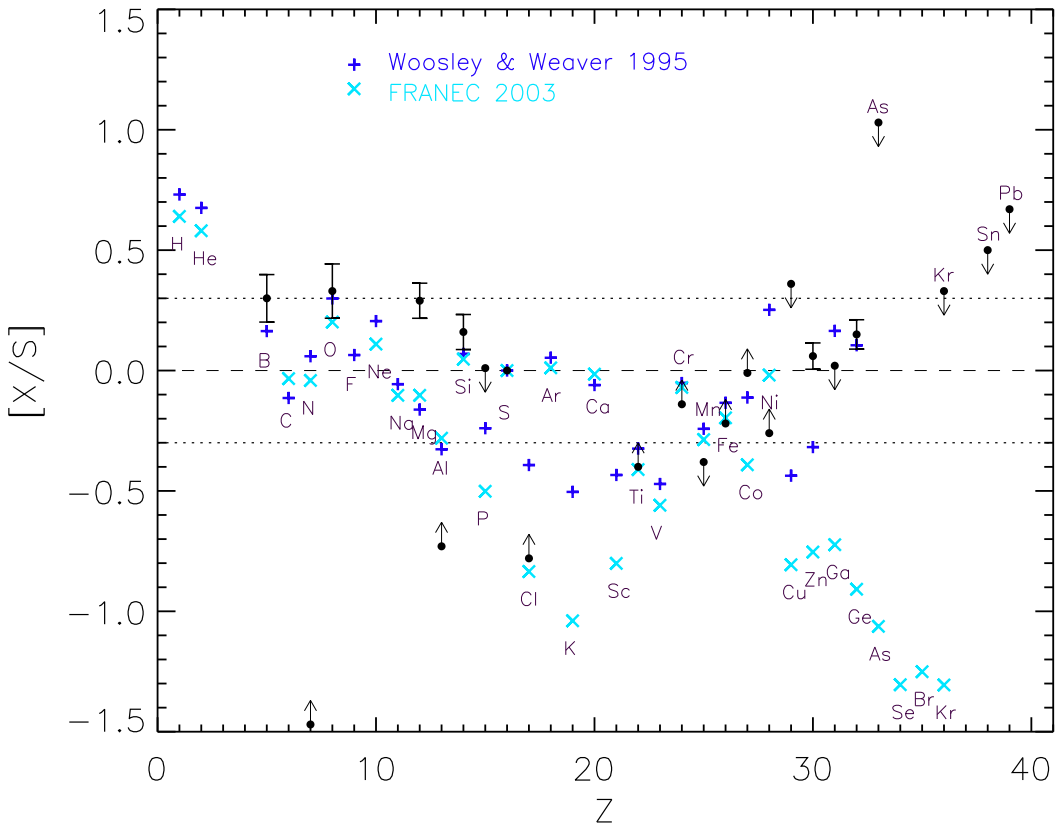


FIG. 6.— Predicted abundance pattern of a 2.2 Gyr object with [O/H] = −0.44 obtained using the Woosley & Weaver 1995 yields (*plus signs*) and FRANEC 2003 yields (*crosses*). Other symbols have the same meaning as in Figure 2.

licities (Fenner et al. 2003).

#### 4.3.3. *Sulfur*

Sulfur was used as the reference element in this study in preference to Fe because its nucleosynthetic origin is thought to be better understood. Hydrostatic burning and explosive O and Si burning in massive stars are the main processes responsible for S production. Although Fe has traditionally been a popular metallicity gauge, owing to easily observable stellar spectral lines, the question of its origin is complicated by the fact that both Type Ia and Type II SNe can make important contributions to the interstellar Fe content. Moreover, the Fe yield from massive stars is subject to uncertainties relating to the SN II mass cut. Oxygen is a common alternative reference element, but due to the recent significant revisions in the solar O abundance, we chose to plot abundance ratios relative to S, which has been detected in a reasonable number of DLAs and local stars.

#### 4.3.4. *Titanium*

Titanium is a curious element given that observationally, it follows the trends of the alpha-elements in nearby stars, but theoretically, is expected to behave as an iron-peak element. There is currently only a lower limit on Ti in this protogalaxy, however one might expect Ti to be enhanced with respect to iron, given the enhancement of O, Mg, and Si. In contrast, the model predicts [Ti/Fe] $\sim$ -0.2 dex. The deficit of Ti generated by standard SN II and SN Ia models is a well-known unresolved problem (e.g. Timmes et al. 1995, Alibes et al. 2001).

#### 4.3.5. *Zinc*

Iron is often used as a metallicity gauge in stellar populations because of the ease with which it can be observed. However, the abundance of iron in gas is difficult to estimate because it is readily incorporated into dust grains (Savage & Sembach 1996). Furthermore, all of the elements comprising the Fe-peak are refractory. Thus Zn has become a popular substitute for Fe in DLA studies because it is largely free from the effects of dust-depletion and because the Zn/Fe ratio in local stars is approximately solar over a wide range of metallicities. The constancy of Zn/Fe vs Fe/H has lead authors to propose that Zn, like Fe, is generated mostly by Type Ia SNe (e.g. Matteucci et al. 1993, Mishenina et al. 2002). However this need not be the case, since the metallicity dependence of Zn production in massive stars can naturally lead to a time delay that mimics that of SN Ia. As can be inferred from Figure 2, Zn yields predicted by the W7 Type Ia SNe model (Iwamoto 1999) are small in comparison to WW95 SNe II yields (whereas the iron-peak elements from V to Ni can be largely attributed to SNe Ia). Figure 3 reveals the strength of the metallicity-dependence of Zn production in massive stars. These effects can combine to allow Zn and Fe enrichment to occur in lockstep despite having different nucleosynthetic origins.

Figure 7 illustrates potential problems associated with using Zn as a proxy for Fe. The four panels plot [S/Fe] (*left panels*) and [S/Zn] (*right panels*) versus time (*upper panels*) and metallicity (*lower panels*). The curves correspond to different radii in a Milky Way-like galaxy. The inner radius has the strongest star formation rate and the earliest peak. Star formation proceeds more slowly with increasing radius. Owing to the delayed release of large amounts of Fe from SNe Ia with respect to the release of S from short-lived massive stars, the behaviour of [S/Fe] (or [O/Fe]) vs [Fe/H] can be used to diagnose star formation histories. Slower and more protracted star formation, such as in the outer disk of a galaxy, should to lead to subsolar [S/Fe] (and [O/Fe]) at lower [Fe/H] (*lower left panel*). But when Fe is replaced by Zn (*lower right panel*), the behaviour at all radii is virtually indistinguishable. This is a consequence of the nucleosynthesis prescriptions adopted in this paper that have Zn being produced mostly by massive stars as an increasing function of initial stellar metallicity. Under this formalism, the evolution of Zn mirrors that of Fe only for certain star formation histories, but might deviate markedly in other environments. Note that it is impossible to attain the solar and subsolar values of S/Zn at the low Zn/H that are observed in DLAs (e.g. Centurión et al. 2000) using the conventional Type Ia and II SNe models employed in this study, regardless of SF history (*lower right panel*). This may indicate a deficiency in our theories of Zn production from the standard SN II and SN Ia nucleosynthesis models. Other authors (e.g. Calura, Matteucci, & Vladilo 2003) have produced low [S/Zn] at low metallicity using chemical evolution models, but they achieve this by ignoring the theoretically predicted SN II and SN Ia Zn yields and instead assume that Zn comes mostly from SNIa and scales with the Fe yield.

There are two main weaknesses of the standard models of Type Ia and II SNe that highlight the uncertainties in the nucleosynthetic origins of Zn: firstly, the models are unable to explain the supersolar values of [Zn/Fe] in metal-poor stars; and secondly, the predicted Zn isotopic composition is at odds with solar. Breaking down the theoretical SNe II Zn yield into its main isotopes reveals substantial disagreement with the solar pattern. The dominant isotope in the Sun is $^{64}$Zn, yet WW95 Type II models underestimate its abundance by a factor of $\sim$3. Conversely, $^{68}$Zn is overproduced by a similar factor. Since the W7 SNe Ia model also underpredicts $^{64}$Zn, other processes might need to be invoked to elevate $^{64}$Zn to solar proportions. The uncertainty regarding zinc's production sites is unfortunate given its key role in diagnosing DLAs.

Neutrino-driven neutron star winds (Woosley & Hoffman 1992; Hoffman et el. 1996) may be an important supplemental site for Zn synthesis. WW95 claim that neutrino winds accompanying the r-process are probably the chief production site of $^{64}$Zn, as opposed to the neutron capture process during helium burning that is included in their SN II models. Alternatively, a blend of fallback and mixing in energetic hypernovae (HNe) have been found to produce $^{64}$Zn in prodigious amounts (Umeda & Nomoto 2002), leading to [Zn/Fe] values compatible with stellar observations. Each of these HNe may eject up to $4\times10^{-4}$ $M_\odot$ of $^{64}$Zn; about ten times more than a typical SN II.

Figure 7 illustrates the tendency for a system with a "burstier" SFH (such as the innermost disk) to maintain elevated [S/Fe] over a wide range of [Fe/H] because the ISM becomes metal-rich before SNe Ia have a chance to dominate Fe production. The age-metallicity relation is gradual in the outer disk, such that for a given [Fe/H], there has been more time for SNe Ia to contribute to the abundance pattern. Thus, the outer radii in Figure 7 reaches [S/Fe] = 0 at [Fe/H] = $-0.7$, whereas the inner radii has [S/Fe] = $+0.2$ at [Fe/H] = $-0.7$. Note however, that in the time domain, it is the slowly forming systems that maintain elevated [S/Fe] for longer temporal periods. Indeed, it takes about 10 Gyr for the outer disk in this model to reach solar S/Fe. This corresponds to a much lower redshift than is characteristic of most DLAs. The DLA population is characterised by roughly solar $\alpha$/Fe values, a mean metallicity $\sim$ 1/10th solar, and ages $\lesssim$ 5 Gyr. According to our standard disk galaxy model, in which the gas infall timescale increases with Galactocentric radius, only the outer regions of the disk can reach [$\alpha$/Fe] $\sim$ 0 at [Fe/H] $\sim -1$, but on timescales $>$ 5 Gyr. In order to get [$\alpha$/Fe] $\sim$ 0 at [Fe/H] $\sim -1$ on sufficiently short timescales one may invoke a short star formation burst of low efficiency (to keep the metallicity down) or a galactic wind that preferentially removes $\alpha$-elements (e.g. Calura et al. 2003). Dwarf

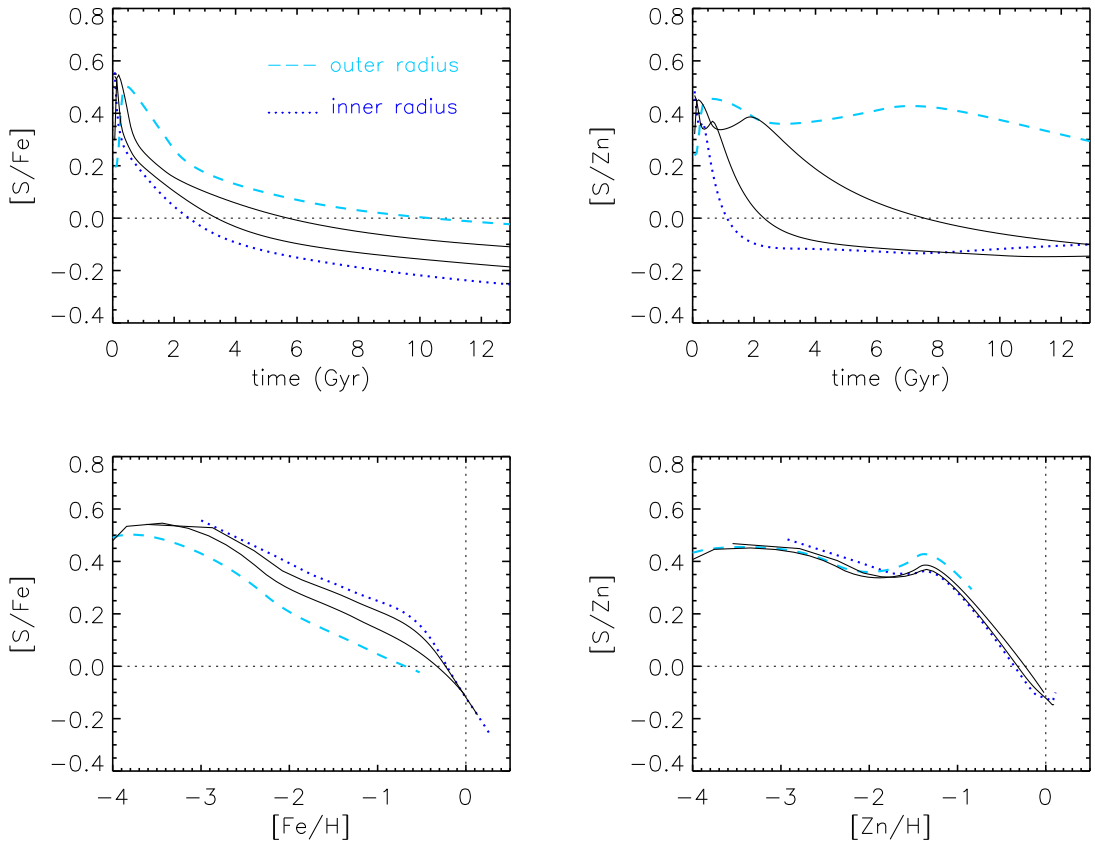


FIG. 7.— The evolution of S relative to Fe (*left panels*) and relative to Zn (*right panels*) as a function of time (*upper panels*) and metallicity (*lower panels*). The four curves in each figure correspond to different radii in a Milky Way-like disk galaxy. The inner radius (*dotted line*) reaches subsolar [S/Fe] quickly owing to earlier and stronger star formation. The outer region of the disk (*dashed line*) is expected to remain enhanced in S and alpha-elements for longer because the drawn-out star formation causes the SNe Ia rate to peak at later times. In [Fe/H]-space the trends are reversed, with the inner disk maintaining supersolar [S/Fe] at higher metallicity because the early intense star formation pushes the gas towards high [Fe/H] before SNe Ia start to dominate Fe production. The upper panels show that only for certain radii does the evolution of Zn resemble that of Fe. Given our adopted SN II and SN Ia nucleosynthesis prescriptions, Zn originates primarily from SNe II with a metallicity-dependent yield. Sulfur also comes mostly from SNe II with a fairly metallicity-independent yield. Thus the curves showing [S/Zn] vs [Zn/H] for various radii overlay one another.

galaxies are more closely associated with these phenomena than disk galaxies.

#### 4.3.6. *Gallium and Germanium*

The predictions from our standard model for the abundance of Ga and Ge are in rough agreement with the data, however we hesitate to draw conclusions based on these results owing to the uncertainties surrounding their synthesis. Although Woosley & Weaver (1995) include Ga and Ge in their tables of yields, they state that the synthesis of all isotopes above $^{66}$Zn are not considered accurate. Indeed, the WW95 Ga and Ge yields are remarkably sensitive to factors including the explosion energy. We also note that WW95 predict a *stronger* metallicity-dependence for the even-numbered Ge than for the odd-numbered Ga (Figure 4).

## 5. SUMMARY AND FUTURE DIRECTIONS

We have predicted the chemical evolution of a DLA as a function of star formation history, age, and metallicity, and find that the enrichment pattern detected in absorption in a $z = 2.626$ protogalaxy is generally consistent with the nucleosynthetic signature of Type II SNe with a moderate contribution from Type Ia SNe. Despite this gratifying agreement with the data, a few inconsistencies remain that may provide insight into nucleosynthetic processes. The underproduction of Mg and Zn with respect to S in our models lends support to an idea already hinted at by discrepancies between the observed abundances in nearby stars and the yields from standard SN II models, that these elements may require additional production sites such as: intermediate mass stars, in the case of Mg; and neutrino-winds, in the case of Zn. It is also likely that tighter constraints on Cl and Cu in the future will see these elements being underproduced by all but the highest metallicity SN II models. This may indicate that the odd-even effect is weaker than predicted by stellar nucleosynthesis models.

DLA-B/FJ0812+32 is expected to soon be complemented by a growing database of detailed abundance patterns of DLAs covering a range of metallicities and redshifts. These observations will represent a new regime for probing chemical evolution in diverse environments with an assortment of enrichment histories. As well as providing further insight into the nature of the DLA population, such a database will complement local stellar observations to help uniquely constrain nucleosynthesis processes. In particular, we await future detections of Cl and P in this and other DLAs. Detection of these odd-elements should enable the SN II models of WW95 and FRANEC to be assessed in terms of their different pre-

dictions for the magnitude of the odd-even effect. We also propose that the detection of s-process elements like Kr and particularly Pb, holds promise as a sensitive measure of the age of intermediate to high redshift DLAs.

Future observations of DLA-B/FJ0812+32 are also expected to yield measurements of C, N, F, Ga, and Sn. Fluorine, like boron, is difficult to measure in stars, but can be detected in absorption in DLAs, providing a test of the $\tau$-process believed to operate during the core-collapse phase of massive stars. It is hoped that Ga measurements will provide insight into the r-process in the early universe. Carbon and nitrogen detections will be especially fruitful because they can be compared against the dataset of N in DLAs and C and N in local stars. Furthermore, knowledge of CNO abundances in a single DLA will constrain theories of nucleosynthesis in intermediate mass stars.

The authors would like to thank A. Wolfe and J.C. Howk for allowing us to present results from the DLA-B/FJ0812+32 observations prior to full publication. We are grateful to Alessandro Chieffi and Marco Limongi for providing their latest stellar yields prior to publication. We wish to thank Stan Woosley for helpful discussions. BKG acknowledges the support of the Australian Research Council, through its Large Research Grant and Discovery Project schemes. We thank the referee P. Bonifacio for his detailed comments that helped improve this paper.

REFERENCES

Alibés, A., Labay, J., & Canal, R. 2001, A&A, 370, 1103
Allende Prieto, C., Lambert, D. L., & Asplund, M. 2001, ApJ, 556, L63
Anders, E. & Grevesse, N. 1989, Geochim. Cosmochim. Acta, 53, 197
André, M. K. et al. 2003, ApJ, 591, 1000
Calura, F., Matteucci, F., & Vladilo, G. 2003, MNRAS, 340, 59
Carigi, L. 2000, Revista Mexicana de Astronomia y Astrofisica, 36, 171
Carretta, E., Gratton, R., Cohen, J. G., Beers, T. C., & Christlieb, N. 2002, AJ, 124, 481
Cayrel, R. et al. 2003, astro-ph/0311082
Centurión, M., Bonifacio, P., Molaro, P., & Vladilo, G. 2000, ApJ, 536, 540
Fenner, Y. & Gibson, B. K. 2003, Publications of the Astronomical Society of Australia, 20, 189
Fenner, Y., Gibson, B. K., Lee, H.-c., Karakas, A. I., Lattanzio, J. C., Chieffi, A., Limongi, M., & Yong, D. 2003, Publications of the Astronomical Society of Australia, 20, 340
Fields, B. D. & Olive, K. A. 1999, ApJ, 516, 797
Gibson, B. K., Loewenstein, M., & Mushotzky, R. F. 1997, MNRAS, 290, 623
Haehnelt, M. G., Steinmetz, M., & Rauch, M. 1998, ApJ, 495, 647
Henry, R. B. C., Edmunds, M. G., & Köppen, J. 2000, ApJ, 541, 660
Hoffman, R. D., Woosley, S. E., Fuller, G. M., & Meyer, B. S. 1996, ApJ, 460, 478
Holweger, H. 2001, AIP Conf. Proc. 598: Joint SOHO/ACE workshop "Solar and Galactic Composition", 23
Iwamoto, K., Brachwitz, F., Nomoto, K., Kishimoto, N., Umeda, H., Hix, W. R., & Thielemann, F. 1999, ApJS, 125, 439
Kroupa, P., Tout, C. A., & Gilmore, G. 1993, MNRAS, 262, 545
Kulkarni, V. P., Fall, S. M., & Truran, J. W. 1997, ApJ, 484, L7
Lanfranchi, G. A. & Friaça, A. C. S. 2003, MNRAS, 343, 481
Langer, N. 1996, ASP Conf. Ser. 112: The History of the Milky Way and Its Satellite System, 169
Le Brun, V., Bergeron, J., Boisse, P., & Deharveng, J. M. 1997, A&A, 321, 733
Limongi, M., Straniero, O., & Chieffi, A. 2000, ApJS, 129, 625
Limongi, M. & Chieffi, A. 2002, Publications of the Astronomical Society of Australia, 19, 246
Limongi, M. & Chieffi, A. 2003, in preparation
Lu, L., Sargent, W. L. W., Barlow, T. A., Churchill, C. W., & Vogt, S. S. 1996, ApJS, 107, 475
Matteucci, F., Raiteri, C. M., Busson, M., Gallino, R., & Gratton, R. 1993, A&A, 272, 421
Matteucci, F. & Recchi, S. 2001, ApJ, 558, 351
McWilliam, A. 1997, ARA&A, 35, 503
McWilliam, A., Rich, R. M., & Smecker-Hane, T. A. 2003, ApJ, 592, L21
Mishenina, T. V., Kovtyukh, V. V., Soubiran, C., Travaglio, C., & Busso, M. 2002, A&A, 396, 189
Nakamura, T., Umeda, H., Nomoto, K., Thielemann, F., & Burrows, A. 1999, ApJ, 517, 193
Nissen, P. E., Chen, Y. Q., Schuster, W. J., & Zhao, G. 2000, A&A, 353, 722
Pettini, M., Ellison, S. L., Steidel, C. C., Shapley, A. E., & Bowen, D. V. 2000, ApJ, 532, 65
Prochaska, J. X. & Wolfe, A. M. 1997, ApJ, 487, 73
Prochaska, J. X. & Wolfe, A. M. 2002, ApJ, 566, 68
Prochaska, J. X. 2003, ApJ, 582, 49
Prochaska, J. X., Howk, J. C., & Wolfe, A. M. 2003, Nature, 423, 57
Prochaska, J. X., Gawiser, E., Wolfe, A. M., Cooke, J., & Gelino, D. 2003, ApJS, 147, 227
Rao, S. M., Nestor, D. B., Turnshek, D. A., Lane, W. M., Monier, E. M., & Bergeron, J. 2003, ApJ, 595, 94
Salpeter, E. E. 1955, ApJ, 121, 161
Savage, B. D. & Sembach, K. R. 1996, ApJ, 470, 893
Schaller, G., Schaerer, D., Meynet, G., & Maeder, A. 1992, A&AS, 96, 269
Schmidt, M. 1959, ApJ, 129, 243
Sheinis, A. I., Bolte, M., Epps, H. W., Kibrick, R. I., Miller, J. S., Radovan, M. V., Bigelow, B. C., & Sutin, B. M. 2002, PASP, 114, 851
Thielemann, F.-K., Nomoto, K., & Yokoi, K. 1986, A&A, 158, 17
Timmes, F. X., Woosley, S. E., & Weaver, T. A. 1995, ApJS, 98, 617
Tinsley, B. M. 1980, Fundamentals of Cosmic Physics, 5, 287
Travaglio, C., Gallino, R., Busso, M., & Gratton, R. 2001, ApJ, 549, 346
Umeda, H. & Nomoto, K. 2002, ApJ, 565, 385
van den Hoek, L. B. & Groenewegen, M. A. T. 1997, A&AS, 123, 305
Vladilo, G. 2002, A&A, 391, 407
Wang, B. & Silk, J. 1993, ApJ, 406, 580
White, R. L. et al. 2000, ApJS, 126, 133
Woosley, S. E. & Hoffman, R. D. 1992, ApJ, 395, 202
Woosley, S. E. & Weaver, T. A. 1995, ApJS, 101, 181